Plasma shape effects on L-H power threshold and H-mode in JET-ILW

E.R. Solano[1], E Delabie[2], F. Rimini[3], R.B. Morales[3], M. Maslov[3], A. Kirjasuo[4], G. Verdoolaege[5], A. Huber[6], L. Frassinetti[7], S. Saarelma[3], M. Chernyshova[8], C. Silva[9], E. Pawelec[10], W. Gromelski[11], S. Menmuir[3], Z. Huang[3], A. Baciero[1], E. de la Luna[1], J.M. Fontdecaba[1], JET Contributors and EUROfusion Tokamak Exploitation Team[†]

[1]Laboratorio Nacional de Fusión, CIEMAT, Madrid, Spain; [2]Oak Ridge National Laboratory, Oak Ridge, USA; [3]UKAEA Abingdon, United Kingdom; [4]University of Helsinki, Finland; [5]Department of Applied Physics, Ghent University, Belgium; [6]Forschungszentrum Jülich GmbH, Institute of Fusion Energy and Nuclear Waste Management-Plasma Physics, Jülich, Germany; [7]KTH Royal Institute of Technology, Stockholm, Sweden; [8]National Centre for Nuclear Research, Otwock, Poland; [9]Instituto de Plasmas e Fusão Nuclear, Lisboa, Portugal; [10]Institute of Physics Opole, Poland; [11]Institute of Plasma Physics and Laser Microfusion, Warsaw, Poland

[†]*See the author list of N. Vianello et al 2026 Nucl. Fusion 66 116010*

In JET-ILW it has been documented that the L-H transition power threshold, P_{LH}, is higher when strike points are at divertor corners (CC), and lower in plasmas with inner strike in the vertical target and outer strike on the central horizontal targets (VH) [1-4]. These configurations are illustrated in Fig. 1. Here we discuss only Deuterium plasmas, and in all cases the plasma has a single null with ion grad-B drift pointing to the X-point.

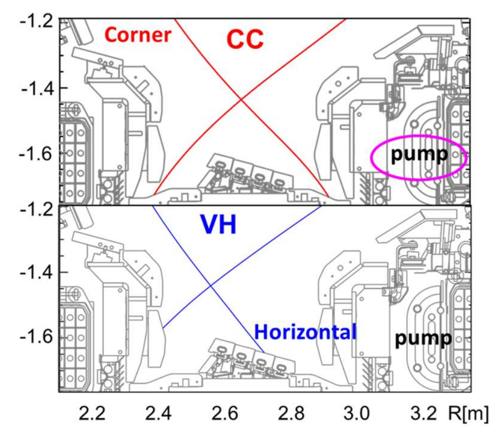

Fig. 1: Corner and Vertical-Horizontal plasma configurations in the JET-ILW divertor

The impact of plasma configuration on P_{LH} is included in the recent multimachine empirical scalings for L-H threshold power (derived from the metal wall tokamaks AUG, C-Mod and JET-ILW) as an overall multiplier **D** [5]. Although confirmed in JET-ILW, the dependence of P_{LH} on plasma shape and even on divertor hardware had already been documented in JET-C [6,7].

Because the tokamak transport equations are written in terms of flux surface averages, confinement is expected to be proportional to plasma current for fixed size [8]. This is in fact confirmed by empirical energy confinement scalings [9] ITER L-96 for L-mode, and IPB98(y,2) for H-mode. Therefore, it isn't surprising that the least scatter for P_{LH} multi-machine scaling is obtained using B_{pol} instead of B_{tor} as a fitting parameter: $P_{L\text{-}H}= 0.167\ \mathbf{D}\ B_{pol}^{0.63} n_e^{1.08}\ S^1\ 2/M_{eff}^1$ [5]. For the B_{pol} P_{LH} scaling, the multiplier factor values are **D**=1 for VH and **D**=1.66 for CC, bringing the largest uncertainty to P_{LH} predictions for future devices.

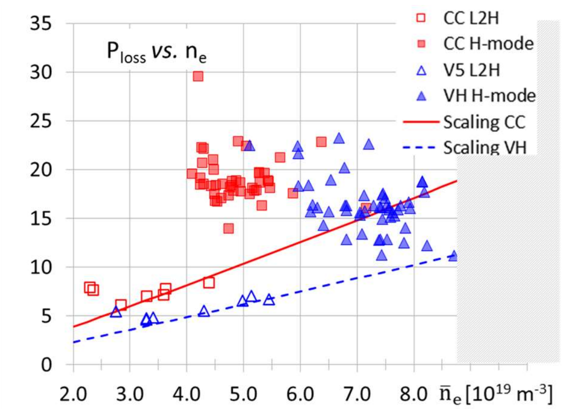

Fig. 2 P_{loss} as a function of $\bar{n}_e$. for L-H transition , scalings and H-modes for 2.5 MA dataset. The dashed area marks f_{GW}>1.

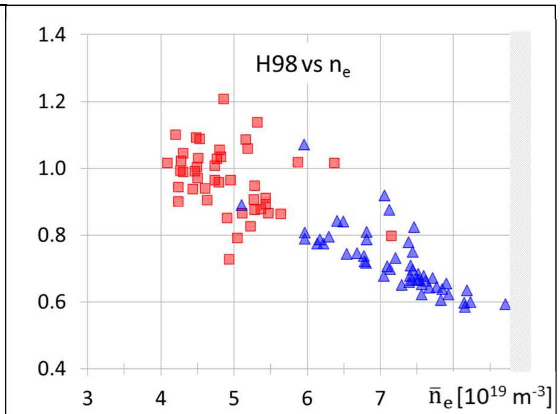

Fig. 3: H-mode confinement factor H98 as a function of $\bar{n}_e$ for 2.5 MA H-modes

Note that **D** cannot be explained by configuration dependence of the measured radial electric field E_r or its shear [10], which in fact has been shown not to provide L-H transition pre-conditions at JET-ILW [11]. Partial detachment and dithers do influence the transition [1] and they can depend on the configuration. Switching off the cryopump has been shown experimentally not to affect P_{LH} for VH. The possibility that CC has higher threshold than VH due to lower L-mode confinement is negated by the JET-ILW L-mode confinement database [12], which shows no configuration effects on τ_E.

In Fig. 2 we show P_{LH} (P_{loss}) threshold data vs. line averaged density for CC and VH (hollow red squares and blue triangles, respectively), together with their corresponding scalings, for 2.5 MA plasmas. Also shown in Fig. 2 are P_{loss} vs $\bar{n}_e$ values for the CC and VH 2.5 MA steady H-modes of the JET-ILW H-mode database, with matching colors but filled symbols [11], showing that in all these H-modes CC plasmas have lower density. Fig. 3 shows the normalized confinement time H98: the good confinement of CC H-modes arises from access to lower density conditions rarely obtained in VH [13,14, 15].

This H-mode configuration effect was first observed in an experiment with constant power and fueling (from the main chamber), with two steady phases CC and VH [16], shown in Fig. 4. The time traces of Fig. 4a show the density rise and drop in pedestal temperature, H98 and plasma energy W_{MHD}, from the change of strike location. In the CC phase the ELMs are periodic type I ELMs, while in VH there are some small ELMs mixed in-between the large type I ELMs. Fig. 4b shows density and temperature profiles for selected times just before and just after type I ELMs in each phase. The higher density of the VH phase is localized outside R=3.5 m, both for pre and post-ELM profiles. The particle loss associated with type I ELMs is larger in VH than in CC., so a change in ELM character doesn't explain the density rise and confinement change. It is presumed that the greater distance between divertor strike point and the cryogenic pump (see location in Fig. 1) leads to a fast refill of the density pedestal in VH when compared to CC.

Shown in the table below Fig. 4 are confinement characteristic in both phases, showing that the ratio P_{loss}/P_{LH} isn't a good indicator of H-mode quality for this case. The lower confinement may be explained in part by the known degradation of energy confinement at higher densities.

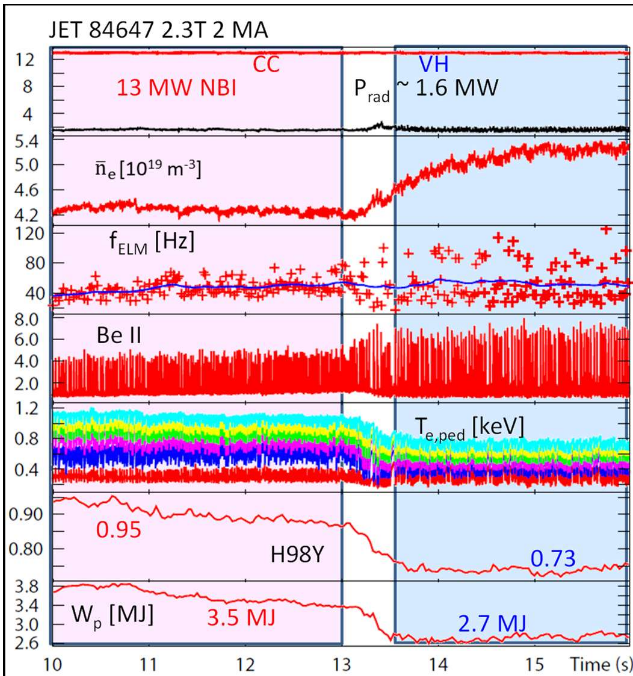

Fig. 4a: Changes in plasma confinement due to motion of strike points from CC to VH.

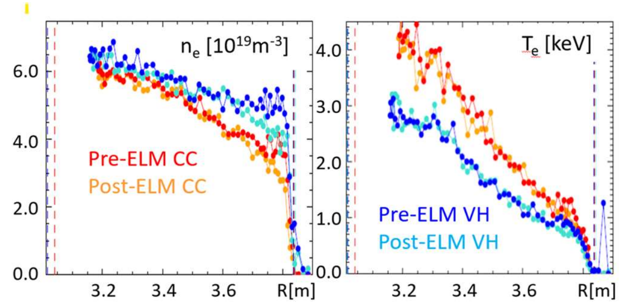

Fig. 4b: Thomson Scattering profiles before and after selected type I ELMs. See legend for colour codes.

Table: confinement characteristics of both phases

	$\bar{n}_e$ [m^{-3}]	H98	P_{loss} [MW]	$P_{LH,scal}$ [MW]	$P_{loss}/P_{LH,scal}$
CC	4.4e19	0.9	13.5	8.2	1.6
VH	5.3e19	0.7	13.5	7.0	1.9

In another example, a deliberate reduction of gas fueling in the VH phase of the pulse leads to constant $\bar{n}_e$ and ELM frequency in both phases, shown in Fig. 5. Despite similar averaged density, pre-ELM profiles shown in Fig. 5 have low $n_{e,ped}$ and high $T_{e,ped}$, and overall hotter core profiles in CC . Impurity charge-exchange measurements show that T_i=T_e in all cases (not shown in plots), and pedestal toroidal ion rotation is about 4 kHz in the CC phase, 2 kHz in the VH phase (higher pedestal density for similar momentum input). In this example the ELMs are of type I in both phases, near the ballooning branch of the peeling-ballooning boundary, and the ELMs in the CC phase erode more W than in the VH, as is too be expected due to the hotter pedestal.

Shown in Fig. 6 are density and temperature profiles before and after typical ELMs, obtained with reflectometry [17] and ECE [18] measurements. A similar number of particles is expelled in each ELM. Again, because in CC the outer strike is near the cryo-pump, we propose the particles

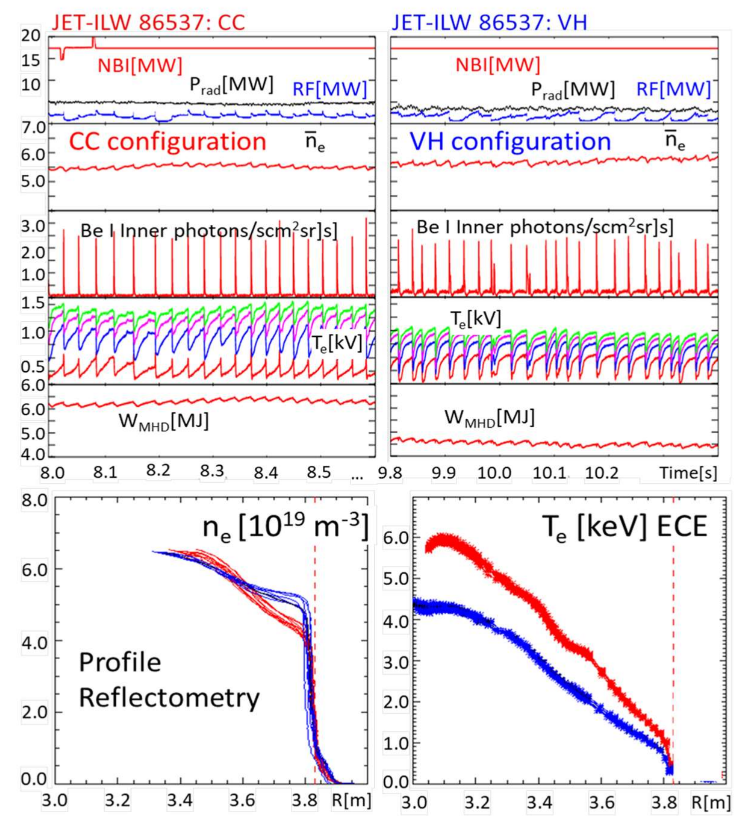

Fig. 5: Pre-ELM plasma profiles from various ELMs, when gas is adjusted to obtain constant $\bar{n}_e$ and f_{ELM} in CC and VH phases, with constant heating power. H98 factors are 1.2 in CC, 0.87 in VH, power ratios are 1.3 for CC, 2.5 in VH.

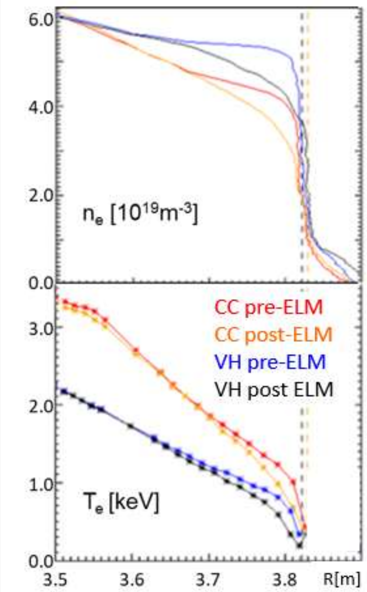

Fig. 6: Pre and post-ELM profiles, see legend for colour codes.

expelled at each ELM are pumped away more effectively, while in VH they are returned to the plasma and sustain higher $n_{e,ped}$, despite the reduced fueling. Modelling of this exhaust mechanism should be possible with modern tools [19,20].

In summary, despite lower P_{LH} in VH configuration, at 2.5 MA good H98 is mostly observed in CC at low densities. $P_{loss}/P_{LH,scal}$ is not a good predictor of ELMy regime or good confinement. For any planned fusion operating regime consider access and stationarity conditions for good overall confinement, different from conditions for low P_{LH}.

References:

[1] E. Delabie et al *25th IAEA Fusion Energy Conf., Saint-Peterburg, Russia, 2014*
[2] C.F. Maggi *et al* *NF 54 023007 (2014)*
[3] E. Delabie et al *42nd EPS Conf. on Plasma Physics, Lisbon, 2015*
[4] E. R. Solano *et al* *NF **61** 124001 (2021)*
[5] E. Delabie et al *NF 66 036016 (2026)*
[6] Y Andrew et al PPCF 46 A87 (2004)
[7] Y Andrew et al 2008 PPCF 50 124053
[8] E.R. Solano *PoP 1, 548–551 (1994)*
[9] ITER Physics Basis 1999 *NF 39 2137*
[10] C. Silva, et al, *NF 62 126057 (2022)*
[11] C. Silva, *this conference*
[12] A. Kirjasuo, *private communication*
[13] M. Maslov *et al* *NF 60 036007 (2020)*
[14] C.F. Maggi *et al* *NF 55 113031 (2015)*
[15] E de la Luna et al., *25th IAEA FEC 2014, ibid.*.
[16] E.R. Solano et al, *41st EPS Conf. on Plasma Physics, Berlin, 2014* P1.006
[17] R. B. Morales, *RSI 95, 043501 (2024)*
[18] E. de la Luna et al, *RSI 75, 3831 (2004)*
[19] P. Tamain et al, *JNM 463 (2015)*
[20] E. Joffrin et al NF 57 086025 (2017)

Acknowledgements: This work has been carried out within the framework of the EUROfusion Consortium, funded by the European Union via the Euratom Research and Training Programme (Grant Agreement No 101052200-EUROfusion). Views and opinions expressed are however those of the author(s) only and do not necessarily reflect those of the European Union or the European Commission. Neither the European Union nor the European Commission can be held responsible for them. Additionally, this research was supported in part by grant PID2021-127727OB-I00, funded by MICIU/AEI/10.13039/501100011033 and by ERDF/EU